Author Manuscript

Author Manuscript

Author Manuscript

Author Manuscript

HHS Public Access

Author manuscript

J Anat. Author manuscript; available in PMC 2016 January 11.

Published in final edited form as:

J Anat. 2015 September ; 227(3): 255–267. doi:10.1111/joa.12343.

The human brain and face: mechanisms of cranial, neurological and facial development revealed through malformations of holoprosencephaly, cyclopia and aberrations in chromosome 18

Marjorie C. Gondré-Lewis[1], **Temitayo Gboluaje**[1], **Shaina N. Reid**[1], **Stephen Lin**[2], **Paul Wang**[2], **William Green**[3], **Rui Diogo**[3], **Marie N. Fidélia-Lambert**[4], and **Mary M. Herman**[5]

[1]Laboratory for Neurodevelopment, Department of Anatomy, Howard University College of Medicine, Washington, DC, USA

[2]Department of Radiology, Howard University College of Medicine, Washington, DC, USA

[3]Laboratory for Evolutionary Biology, Department of Anatomy, Howard University College of Medicine, Washington, DC, USA

[4]Department of Pathology, Howard University College of Medicine, Washington, DC, USA

[5]Clinical Brain Disorders Branch, National Institute of Mental Health, National Institutes of Health, Bethesda, MD, USA

Abstract

The study of inborn genetic errors can lend insight into mechanisms of normal human development and congenital malformations. Here, we present the first detailed comparison of cranial and neuro pathology in two exceedingly rare human individuals with cyclopia and alobar holoprosencephaly (HPE) in the presence and absence of aberrant chromosome 18 (*a*Ch18). The *a*Ch18 fetus contained one normal Ch18 and one with a pseudo-isodicentric duplication of chromosome 18q and partial deletion of 18p from 18p11.31 where the HPE gene, TGIF, resides, to the p terminus. In addition to synophthalmia, the *a*Ch18 cyclopic malformations included a failure of induction of most of the telencephalon – closely approximating anencephaly, unchecked development of brain stem structures, near absence of the sphenoid bone and a malformed neurocranium and viscerocranium that constitute the median face. Although there was complete erasure of the olfactory and superior nasal structures, rudiments of nasal structures derived from the maxillary bone were evident, but with absent pharyngeal structures. The second non-*a*Ch18 cyclopic fetus was initially classified as a true Cyclops, as it appeared to have a proboscis and one median eye with a single iris, but further analysis revealed two eye globes as expected for synophthalmic cyclopia. Furthermore, the proboscis was associated with the medial ethmoid ridge, consistent with an incomplete induction of these nasal structures, even as the nasal septum and paranasal sinuses were apparently developed. An important conclusion of this study is that it is the brain that predicts the overall configuration of the face, due to its influence on the development of

Correspondence Marjorie C. Gondré-Lewis, Associate Professor, Laboratory for Neurodevelopment, Department of Anatomy, Howard University College of Medicine, 520 W Street, NW, Washington, DC 20059, USA. T: +202 806 5274; mgondre-lewis@howard.edu.

Ethical approvals

This article does not contain any studies with human participants or animals performed by any of the authors.

Author Manuscript Author Manuscript Author Manuscript Author Manuscript

surrounding skeletal structures. The present data using a combination of macroscopic, computed tomography (CT) and magnetic resonance imaging (MRI) techniques provide an unparalleled analysis on the extent of the effects of median defects, and insight into normal development and patterning of the brain, face and their skeletal support.

Keywords

holoprosencephaly; HPE; trisomy 18; cyclopia; chromosome 18; neurocranium; viscerocranium; synophthalmia; Edwards'; syndrome; SHH; Pax6; TGIF; craniofacial anomalies; eye development; nose development

Introduction

Proper human development requires interdependent inductive cascades during critical periods of embryonic life. A prime example is the tightly regulated physical and functional relationship of the brain and neurocranium (Richtsmeier & Flaherty, 2013; Reid et al. 2015). The brain develops in synchrony with both the neurocranium and the viscerocranium, but less directly with the muscles of the face. Abnormal development of this brain–cranium–face triad could be caused by a number of factors, including exposure to teratogens such as alcohol, but may also be due to single gene mutations and abnormal chromosomal numbers (Solomon et al.2010; Kietzman et al. 2014). Chromosomal trisomies are well documented to cause malformations (Smith et al. 1960; Cohen, 2002), with increased severity depending on whether shorter vs. longer chromosomes are implicated (i.e. Chr 13 > 18 > 21).

Trisomy 18 (T18), or Edwards' syndrome, is dubbed the second most prevalent trisomy behind Down syndrome (Trisomy 21), and occurs in 1/6000 births (Cereda & Carey, 2012) with fewer than 10% of diagnosed cases surviving to the age of 1. (Rasmussen et al. 2003). Typically, neonates with T18 may present clinically with stunted growth, heart defects, overriding fingers, low-set ears or craniofacial defects (Bruns & Campbell, 2014). If fetuses present with holoprosencephaly (HPE) *in utero*, they will likely not survive, and T18 is a prominent underlying cause of HPE (Aruna et al. 2013). HPE is a midline defect primarily affecting anterior neural tissue, which results in incomplete separation of the forebrain into two individual hemispheres during the third and fourth week of gestation. This impaired patterning of the midline extends to the surrounding neural crest and to mesodermally derived sclerotomes and myotomes, causing severe neurological deficiencies and craniofacial dysmorphisms (Arnold & Meiselbach, 2009; Rosa et al. 2013; Petryk et al. 2015). In the worst cases, the dysmorphogenesis can present as alobar HPE where there is complete fusion of the two hemispheres, with a cyst-like structure in the forebrain from unseparated ventricles, and cyclopia with/without a proboscis (single nostril nasal structure above the orbit) (Lang et al. 1976; Orioli et al. 2011).

In 1964, DeMeyer et al. concluded that faces with median anomalies that feature cyclopia, orbital hypotelorism, a proboscis, or bilateral cleft lip combined with a flat nose and hypotelorism, will predict the presence of an alobar HPE brain (DeMeyer et al. 1964); milder manifestations of hypotelorism can indicate lobar HPE (DeMeyer et al. 1964; Raam et al. 2011). Today, these craniofacial malformations and indeed HPE, can be linked not

Author Manuscript Author Manuscript Author Manuscript Author Manuscript

only to ‘entire’ or ‘partial’ chromosomal duplication problems during meiosis or mitosis, but could specifically be due to ‘individual mutations’ in approximately 12 genes (Roessler et al. 1996; Keaton et al. 2010), the four most prevalent of which are routinely tested, namely: Sonic Hedgehog (SHH) found in 12% HPE, Zinc Finger Protein of Cerebellum (ZIC2) in 9% (Roessler et al. 2009), Sine Oculis Homebox, Drosophilla, Homolog of 3 (SIX3) in 5% and Transforming Growth-Induced Factor (TGIF) in about 2% HPE. Thus, in chromosomal aneuploidies like T18, HPE genes could contribute to midline defects either directly because they are coded for on that chromosome, or indirectly because they function downstream of genes located on the abnormal chromosome.

Studies of congenital malformations are crucial for the understanding of not only normal human development, but also of common variations occurring in the normal human population (Alberch, 1989). For this reason, in the last decades there has been a renaissance of developmental studies on congenital malformations, but most of these studies are done in non-human model organisms, such as mice, chicken or zebrafish. A particularly original aspect of the present work is that it is the first detailed anatomical analysis of brain, neurocranium, viscerocranium, and face in control and cyclopic HPE humans with different types of genetic or chromosomal and without a chromosome 18 defect. Importantly, the current findings strongly support the idea that it is the brain that predicts the face by its influence on the development of skeletal structures. Apart from its implications for the understanding of the development of the normal human phenotype and of common variations, this research on extreme cases is also relevant to understanding specific pathologies due to failure of inductive mechanisms at the earliest stages of development.

Materials and methods

Specimens

The cadaveric materials used are not governed by national or institutional human subject research regulations; nevertheless, all efforts were expended to abide by regulations governing the handling of research materials at the University. There were five human cadaveric specimens analyzed for this study: a 29-week control fetus, two newborn infants with normal appearing craniofacial features, a 28-week partial T18 fetus with cyclopia and alobar HPE [aberrant chromosome 18 (*a*Ch18)], and a 35-week cyclopic fetus with normal karyotype and alobar HPE (non-*a*Ch18). The causes of death of the three control fetus/newborns are unknown, and neuropathological exams were unremarkable. Thus, they were used as non-cyclopic, non-HPE controls.

Fetal age determination

The age of the *a*Ch18 fetus was readily available: based on the last menstrual period of the mother, the gestational age was estimated at 28 weeks. The other specimens were staged for gestational age using the fetus crown–rump length, and hand/toe nail length as they correlate with different developmental stages per the criteria set forth by M. England (England, 1996). By this methodology one fetus was determined to be 29 weeks and designated for age-matched control for the 28-week *a*Ch18 fetus. Another fetus, the non-*a*Ch18 cyclops, was

Author Manuscript Author Manuscript Author Manuscript Author Manuscript

determined to be 35 weeks, and the newborns were known to be within 1 week of birth and used as a control for the 35-week cyclops.

Magnetic resonance imaging (MRI)

The MRI procedure was performed on a GE Signa HDxt 3.0T High-Field System (General Electric Company, CT, USA) using a GE Signa HDxt 3.0T HD knee coil (General Electric Company). T1- and T2-weighted scans were acquired in the sagittal, axial and coronal planes. An additional axial scan was acquired for the *a*Ch18 sample, focusing on the optic nerve. The T1-weighted scans were acquired using a Fluid Attenuated Inversion Recovery (FLAIR) sequence, and the T2-weighted scans were acquired with both FLAIR and Fast Spin Echo sequences.

Computed tomography (CT)

Computed tomography images were acquired using a GE Light-Speed VCT system (General Electric Company). For each specimen, a scan was acquired consisting of at least 80 contiguous 3.75 mm slices, 15 × 15 cm field of view, 512 × 512 matrix, 120 kVp, 80 mAs. Identification of structures from radiographs of MRI and CT was aided by the *Atlas of Clinical Gross Anatomy* (Moses et al. 2005).

3D reconstructions

To analyze craniofacial bones and their features in 3D, image stacks of the CT scan images were initially analyzed with NIH ImageJ software with a 3D plug-in, and final reconstruction was with the 3D slicer software using the Volume Rendering module (Fedorov et al. 2012). Adjusting the image intensity threshold for the dense bones allowed for bone only reconstruction. A lower threshold allowed for reconstruction of soft tissues. Additional 3D reconstructions were performed with the vct system software.

Dissections

To analyze the gross brain, standard gross dissection employing microdissection tools was used. The calvarium was carefully opened using scissors, and the brain and brainstem were removed by adjusting instructions provided in Grant's Dissector (Tank, 2013). A Nikon camera was used to photograph macroscopic structures.

Results

Superficial face and clinical findings in aCh18 cyclopia

By 28–29 weeks of gestation, many features of the normal developing face were already defined. Importantly, sensory organs such as the nose, eyes, ears and tongue of fetuses at this stage were discernibly typical of the expected features of a normal baby (Fig. 1). In the stillborn 28-week fetus described here, superficial features of the face were severely malformed, resulting in absence of the forehead, a single eye orbit and fused eye globes, classically defined as cyclopic. There were no nasal structures except for a small protrusion below the orbit, construed here as the rudiments of the nasal spine. Surprisingly, there was no proboscis, a nasal appendage typically located above the central eye of cyclopic cases

Author Manuscript Author Manuscript Author Manuscript Author Manuscript

(McGrath, 1992). The mouth opening was much narrower than the control and the jaw was micrognathic, but there was no single or bilateral cleft lip (Fig. 1). Other phenotypes included hirsutism (also observed in the trunk), corneal opacity and the 'strawberry skull' deformation typical of patients with Edwards' syndrome (Nicolaides et al. 1992; Ettema et al. 2010). The fetus was also diagnosed with alobar HPE, and the autopsy report cited hypoplastic adrenal glands, ventricular septal defect of the heart and acute involution of the thymus. These organ features have also been reported in patients with T18.

To determine the genetic cause of the observed phenotype, tissue was referred to Quest Diagnostics for genetic testing, and was found to be a duplication of the entire chromosome 18 q (the long arm) and a deletion of nearly the entire short arm, consistent with a pseudo-isodicentric chromosome 18 at about 18p11.31, and thus it was determined that the anticipated clinical spectrum of the child would have been that of Edwards' syndrome, i.e. T18. This specimen is exceedingly rare, as a review of the literature indicates very few cases of chromosomal defects at Ch18 due to translocations or the described specific pseudo-isodicentric chromosome 18 defect (Floore et al. 1989; Gravholt et al. 1997), and rarer still are cases involving both T18 and the presentation of cyclopia with HPE (Lang et al. 1976; Floore et al. 1989).

Brain structures in a*Ch18 cyclopia*—To assess the extent to which 'alobar' HPE affected development of specific brain structures, MRI scans of the fetus in coronal, horizontal and sagittal planes were analyzed. Figure 2A,C shows a significant reduction of the cranial vault, with empty space anteriorly, dorsally and laterally in the telencephalon where there ought to have been neural structures as in the control fetus (Fig. 2B,D). In fact, the cerebral cortex had features more consistent with anencephaly than alobar HPE. Brain stem structures were formed, but were significantly enlarged compared with control (Fig. 2C vs. D). The cerebellum was reduced and no tentorium was perceivable, thus no clear separation between the cerebellum and the telencephalon was present. Although neither the lateral ventricles nor the third ventricle were present, what appears to be a non-communicating aqueduct connected the midbrain with the fourth ventricle. Thus, the defect in induction of neural structures was very severe anteriorly, resulting in absence of the cerebral cortex with more caudal regions being abnormally large and fused.

Gross brain and blood vessels in a*Ch18 cyclopia*—The brain and spinal cord of the *a*Ch18 case were removed from the cranial cavity for additional analysis. Consistent with the MRI images in Fig. 2, there was very little cortex, and nearly a complete absence of the telencephalon compared with control (Figs 2 and 3). Although tissue fixation was attempted, neural structures remained relatively soft and translucent. Most brain material consisted of brainstem, and a midbrain/diencephalon mass of tissue with no hemispheric separation, as well as aplastic falx cerebri and cerebelli. Consistent with the presence of the brainstem, the blood vessels consisted of a well-formed basilar artery traversing the pontine surface, extending from bilateral vertebral arteries to the posterior cerebral artery. Beyond the brainstem, the vasculature was blunt-ended with no apparent Circle of Willis, i.e. no input from the internal carotid artery, and thus no anterior or middle cerebral arteries (Fig. 3).

Author Manuscript Author Manuscript Author Manuscript Author Manuscript

Eye structures in a*Ch18 cyclopia*—The MRIs reveal features consistent with synophthalmic cyclopia in that there were two microphthalmic eye globes fused along the sclera resembling a large single globe (Fig. 4A,B), unlike the age-matched control with the expected individual globes in two separate orbits, separated by nasal structures (Fig. 4C). A midline sagittal section shows a single fused optic nerve entering the brain centrally, rather than laterally, as would be expected in normal development (Fig. 4A, arrow). Consistent with synophthalmic cyclopia, adjacent sections demonstrated no optic nerve, but there were two spaces housing the vitreous humor of each eye on either side of the midline. Although each eye had sclera and vitreous humor, no lens or other anterior chamber structures were detected. The previous analysis of the limb and head musculature of this specimen, which included the extraocular muscles, revealed the absence of the medial rectus as well as the superior and inferior obliques (Smith et al. 2015). Rather, the superior rectus was doubled and a single inferior rectus was present. These MRI analyses confirm the presence of a left and right lateral rectus muscle, and medially located rectus muscles (Fig. 4B).

Nasal and pharyngeal structures in a*Ch18 cyclopia*—In facial malformations with arhinia, a complete absence of nasal structures is expected. Thus, it was surprising to find putative internal nasal structures in the *a*Ch18 cyclopic fetus: the nasal septum, conchae (inferior and middle, but not superior) and, more laterally, the putative maxillary sinuses were formed (Fig. 5). The nasal septum was sandwiched between the central orbit and the hard palate instead of the cribriform plate of the ethmoid bone and the hard palate (Fig. 5, coronal). In the oral region, most of the pharyngeal structures were absent; namely, oropharynx, laryngopharynx and the esophagus as seen in Fig. 5, bottom panel. The alveolar process of the maxilla was aplastic as compared with the normal morphology shown in the control.

Bone morphology of the cranium in a*Ch18 cyclopia*—To analyze the resulting morphology of cyclopia and alobar HPE on the bony features of the human face and neurocranium, 3D reconstructed CT scans of the *a*Ch18 subject were analyzed compared with the control. The frontal, parietal and occipital bones were formed, but as previously reported in other severe cases of midline malformations, the metopic suture of the frontal bone was absent. This was accompanied by a single, significantly smaller frontal bone medially shifted such that the coronal sutures were perceivable from the anterior view, as compared with two separate bones extended more laterally in the control at this stage of fetal development (Fig. 6, anterior). In fact, all of the bones that arise in whole or in part from the neurocranium showed abnormalities. There was, as discussed in Fig. 1, a single orbit, but the reconstructions revealed that this orbit had no floor or roof, as the greater and lesser wings of the sphenoid bones were absent (Fig. 6, anterior view). The defect in the sphenoid bone was drastic, consisting of a suspended plate presumably held together with connective tissue, containing a single optic foramen. The nasal bone was absent altogether along with all the bone processes around it, i.e. the maxillary process (MXP) of the frontal bone and frontal process of the maxillary bone (Fig. 6, anterior). For bone derived from the viscerocranium, there were primarily medial abnormalities such as an aplastic frontal process of maxilla, a highly obtuse mandible with no angle and an absent mental protuberance. More laterally, the zygomatic bone appeared to be normal, as well as the

Author Manuscript Author Manuscript Author Manuscript Author Manuscript

mandibular rami and articulations (Fig. 6, lateral and angled anterior). The posterior view of the 3D reconstructions showed a larger than normal posterior fontanel in the *a*Ch18 subject (Fig. 6, posterior). The posterior cranial bone was present, and the articulating facets of the atlas and axis vertebrae were there; however, more medial supporting structures were not detected. This anteriorly opened cervical vertebra reflects the enlarged foramen magnum and brainstem structures that developed without normal physical constraints from the tight fit of the vertebrae around neural structures (Fig. 2).

Auditory structures in a*Ch18*—Although the bone morphology of the cranium was anomalous, the more laterally located external auditory structures such as the pinna seemed fully developed with typical features. The middle ear ossicles and inner ear cochlea compare closely with the control structures, but were comparatively radiodense as assessed with both MRI and CT analysis (Fig. 7). These results are consistent with the previously reported enlarged petrous portion of the temporal bone and its foramen in the interior of the cranium (Reid et al. 2015), indicating that sensory processing of sound may have been impaired.

Craniofacial features of a non-aCh17 true cyclops

A true cyclops (cyclopia perfecta) is defined as having a nasal appendage, or proboscis, above one median eye lodged in a single orbit, with no nasal structures (Garzozi & Barkay, 1985; Deftereou et al. 2013). The findings in the *a*Ch18 HPE cyclops above were compared with a 35-week fetus fitting the definition of cyclopia perfecta. On the surface, this baby exhibited all expected features of a true cyclops (Fig. 8A,D). However, more careful macroscopic and MRI analysis revealed ocular features more closely associated with synophthalmic cyclopia, as in the *a*Ch18 case, with two separate eye globes surrounded by sclera and fused medially in a single orbit (Fig. 8B,D inset,E). Additionally, both the *a*Ch18 and non-*a*Ch18 specimens exhibited a flat facial profile (Figs 1 and 8C). Each cerebral hemisphere was expanded laterally with cortical tissue (Fig. 8E), but the boundaries of the cortical gray and white matter were not delimited (Fig. 8E vs. F). There was also a single continuous cerebral ventricle spanning the two hemispheres causing a lack of interhemispheric division (8H). Interestingly, some initially fused structures bifurcated to communicate left/right information to the brain when entering the neurocranial cavity (Fig. 8E, arrows), whereas they originated from two lateral orbits as expected in controls (Fig. 8F). Furthermore, much like in the *a*Ch18 subject, the maxillary sinus and rudiments of the nasal conchae were detectable (Fig. 8G).

Analysis of the viscerocranium and neurocranium of the 35-week cyclops revealed that the frontal bone was unitary with no metopic suture (Fig. 9A). Unlike the *a*Ch18 specimen, the orbital plates were partially formed with an ethmoidal notch where the crista galli of the ethmoid bone normally resides (Fig. 9B); thus, unlike the *a*Ch18 cyclops, there was no direct contact between neural structures in the cranial cavity and the underlying eye (Reid et al. 2015). At the point of the base of the proboscis (Fig. 8), there were two bony protrusions from the frontal bone, which would likely give rise to the superior and medial boundaries of the orbit (Fig. 9A). The body, lesser and greater wings of the sphenoid bone were far less rudimentary compared with *a*Ch18, displaying a distinguishable body of the sphenoid even as the wings were diminutive compared with the expected normal state. A single medial slit

Author Manuscript Author Manuscript Author Manuscript Author Manuscript

replaced the two expected optic canals (Fig. 9A). Nonetheless, the sphenoid wings were sufficiently developed to form the boundaries of two bilateral superior orbital fissures (Fig. 8C, arrows). The frontal bone was stunted compared with control (Fig. 9B), and the sphenoid bone was underdeveloped and it, along with the entire middle cranial fossa, was shifted anteriorly as previously shown for the *a*Ch18 cranial fossa (Reid et al. 2015). Lateral perspectives (Fig. 9C) indicated no remarkable lateral abnormalities associated with the face, although there were clear malformations of the bony skeleton related to the occipital bone and the cervical and thoracic vertebrae. Figure 10 emphasizes the presence of maxillary nasal structures that developed in spite of the undescended nose, and undeveloped nasal bone and frontonasal prominence.

Discussion

Much about the normal course of development and its variants in the normal human population can be learned from genetic/genomic errors that lead to congenital malformations. In this study, a very rare case of a human with features consistent with T18 with HPE and synophthalmic cyclopia was analyzed and compared with a non-T18-associated human cyclopic fetus in order to uncover interdependent mechanisms during development. A detailed multi-pronged radiographic imaging analysis is provided of brain, neurocrania and viscerocrania, as well as muscle and soft tissue that make up nasal and pharyngeal structures. The craniofacial anomalies associated with alobar HPE – missing or fused lateral ventricles, aplastic telencephalon (Arnold & Meiselbach, 2009; Aruna et al. 2013) – were detected to varying degrees in the two cyclopic specimens. The facial anomalies in the *a*Ch18 cyclops were centered along the mid-facial line resembling a bilateral medial shift in a manner that erased the most medial neurocranium- derived structures, such as the metopic suture, ethmoid, sphenoid and indeed the nasal bones, and to a lesser extent the viscerocranium-derived maxilla and mandible but not the more laterally located zygomatic bone. A prominent finding here is that absence of external nasal structures and the cribriform plate of the ethmoid bone does not predict the presence or absence of internal nasal structures.

It was further shown that the development of neural tissue dictates development of brain vasculature. Importantly, the study of these two cyclopic specimens reveals that the severity of craniofacial anomalies may be wholly dictated by the extent to which development of the anterior brain was impacted. The HPE brain and co-presenting dismorphic face likely result from abnormal signaling of the prechordal plate, the midline mesendodermal region anterior to the notochord that functions as a head organizer, and is necessary for the survival of neural crest cells emanating from the early forebrain (Aoto et al. 2009). The prechordal plate produces molecular signals such as SHH that sets the median line for the face, patterns the forebrain into two separate hemispheres, and separates the eye fields into two. Thus, abnormal or lack of signaling from the prechordal plate of the future cyclops as early as during neurulation likely impaired the prosencephalic and facial differentiation process during gastrulation (O'Rahilly & Muller, 1989; Solomon et al. 2010), as has been shown experimentally in rodents. The non-*a*Ch18 cyclops resembles classic HPE/cyclopia from a more localized gene deletion, whereas the chromosomal defect in the T18-like cyclops likely recruits a complex series of cascades that become defective. The *a*Ch18 individual has a

Author Manuscript Author Manuscript Author Manuscript Author Manuscript

deletion from p11.31 to the p terminal of chromosome 18, encompassing the Transforming Growth Factor Beta (TGFb) Inducing Factor (TGIF) 1 and TGIF2 loci, and it has been shown that TGIF1 heterozygous loss-of-function mutations are sufficient to induce HPE. In studies by Taniguchi and colleagues (Taniguchi et al. 2012), knocking out TGIF1 and TGIF2 induced HPE-like phenotypes similar to SHH-null embryos, and this absence of TGIF reduced expression of SHH in the forebrain, and upregulated Gli3, a protein that antagonizes the function of SHH. This implies that a functional loss of TGIF is sufficient to induce severe defects in SHH signaling, critically important in mechanisms involving the growth, differentiation and patterning of the developing central nervous system and craniofacial structures (Ingham & McMahon, 2001). This functional loss can occur in T18, where there are three copies of the gene. Furthermore, TGIF regulates the inductive effect of retinoic acid on gene expression. Loss of function of the TGIF gene has been shown to alter gastrulation and, in varying degrees, to induce HPE (Powers et al. 2010), quite likely by influencing other HPE genes such as SHH. Of course, there are probably other mechanisms related to the duplicated regions that could also explain the finding of HPE as it relates to the clinical spectrum of Edwards' syndrome. Additional studies using a more sensitive technique, such as the microarray-based comparative genomic hybridization, are necessary for a more detailed analysis of the full range of genetic defects associated with this chromosomal abnormality.

Synophthalmia and eye development

Failed separation of the eye fields could result in partial or complete fusion of the eyes. In addition to that received from the prechordal plate, the eye receives inductive contributions from neuroectoderm, surface ectoderm, neural crest cells, and mesoderm. After induction at the end of week 3, a pair of optic vesicles emerges from neuroectoderm on either side of the presumptive diencephalon of the forebrain. The optic vesicle grows and forms an optic cup at the point of contact with surface ectoderm. This contact by the optic vesicle reciprocally induces surface ectoderm to invaginate, ultimately detaching, forming the future lens, a process intimately influenced by chorda mesoderm. Whereas SHH at the prechordal plate is crucial for the separation of the single eye field into two optic primordia and in governing the transition from optic vesicle to optic cup, actual induction of eye development specifically requires Pax 6 (Mathers et al. 1997; Carbe et al. 2013). Based on the observations in both the *a*Ch18 and non-*a*Ch18 cyclops, PAX6 signaling likely remained intact or was compensated for during initiation, because eye formation was induced; however, in both cases SHH transcription and protein expression were likely significantly reduced, resulting in synophthalmia.

The current study suggests that the development of the surrounding bones of the orbit may be less reliant on optic globe development *per se* but, rather, on inductive signals from the overlying brain. Although the synophthalmic phenotype seemed identical in both *a*Ch18 and non-*a*Ch18 cyclopic cases, the bones of the orbit contributed by the frontal and sphenoid bone were absent in *a*Ch18 where there was little to no forebrain but, by contrast, were more well formed in the non-*a*Ch18 cyclops, where prosencephalic cortex was fully induced.

Author Manuscript Author Manuscript Author Manuscript Author Manuscript

Development of the face

As a master organizer, the prechordal plate influences induction of both brain and face. Early in the fourth week of gestation, outgrowth and patterning of the five facial primordia are evident around the primitive mouth. The ectoderm and its associated placodes, the brain and axial mesoderm, and the cranial neural crest cells all contribute both inductive and positional information to the face (Couly et al. 1993). SHH is expressed in the ectoderm of the frontonasal processes (FNPs) and MXPs, which, respectively, give rise to the upper and mid-face, and is essential for their morphogenesis (Wall & Hogan, 1995; Belloni et al. 1996; Chiang et al. 1996; Roessler et al. 1996; Helms et al. 1997). Disrupting SHH signaling in the FNP or MXP interrupts their outgrowth, resulting in hypotelorism or clefting between the primordia, as in cleft lip/palate (Hu & Helms, 1999). This is consistent with experiments in animal models where SHH dosing causes variations in facial growth and shape in vertebrates (Young et al. 2010).

SHH present in one tissue (e.g. notochord and prechordal plate) can induce SHH in an adjacent tissue (e.g. floorplate of the neural tube; Marti et al. 1995; Ericson et al. 1996) and, during ontogeny, the future face is well positioned for SHH inductive signaling from the ventral forebrain and from the developing eye (Rubenstein & Beachy, 1998; Kish et al. 2011). Absence of signals from the forebrain is responsible for abnormal development of facial primordia, particularly the frontonasal prominence because blocking SHH prevents its induction in the ventral forebrain, and its subsequent induction in the frontonasal ectodermal zone, a signaling center that regulates facial development (Marcucio et al. 2005; Petryk et al. 2015). The HPE cases in this study both show severe forms of this FNP disruption, as well as malformations of the MXP and other derivatives of the pharyngeal arches and neural crest cells. Associated deformities in craniofacial muscles were also detected: for example, fused medial muscles of the face resulted in one large orbicularis oculi, and an occipitalis muscle fused with the trapezius and sternocleidomastoid which, in turn, were fused with each other (Smith et al. 2015).

Nasal and pharyngeal structures

Much like the distal nose, the proboscis of the 35-week human cyclops is fibrous, cartilaginous and skin-covered, and has a cavity lined with squamous epithelium, olfactory and respiratory mucosa, and with an opening in its distal end (McGrath, 1992). Its base extends to the ethmoidal notch to contribute to the floor of the anterior cranial fossa and the roof of the median orbit.

Both the normal nose and the cyclopic proboscis develop separately from viscerocranium-derived nasal structures. These superior structures develop from the nasal placode and pit medially and anteriorly at the juncture with the developing frontal bone. During development they migrate between the eyes to meet with maxillary nasal structures to form the complete nasal apparatus.

In the *a*Ch18 case, it is evident that the frontonasal prominence, which is influenced by the forebrain, is severely compromised, resulting in no formation of the nasal bridge or the crest and tip of the nose. However, in the non-*a*Ch18 individual, there was partial development of

Author Manuscript Author Manuscript Author Manuscript Author Manuscript

the FNP by virtue of the proboscis, ethmoidal notch and orbital plate. In both cases, rudiments of MXP-derived nasal structures were evident and, in the non-*a*Ch18 cyclops, a well-developed septum was detectable (Fig. 10). It is interesting that the conchae and nasal septum persist, but this may be due to the fact that the nasal septum is derived from tissue between the choanae and is influenced by its contact with the elevation of the palatal shelves as the tongue descends (Steding & Jian, 2010). These data support the initially independent induction of these MXP structures from those of the FNP. Another important finding in the *a*Ch18 was a lack of development of pharyngeal structures, including the nasopharynx, the oropharynx or laryngopharynx, and is consistent with defective patterning of the pharyngeal arches. These defects together with the septal heart defects, hypoplastic adrenal glands and involution of the thymus implicate the influence of SHH along the entire neuraxis, and on the neural crest cell-derived mesenchyme which influence and/or give rise to aspects of these structures.

Conclusion

The two cyclopic HPE cases presented in this paper are at the extreme spectrum of aberrant patterning, but provide insight into the role of TGIF- and/or SHH-mediated signaling by the prechordal plate and notochord for the development and differentiation of median structures in the brain, skull and face. This study stresses how inductive processes involved in formation of these structures are very complex and modular, but at the same time interdependent, emphasizing the delicate links between modularity and integration in development and evolution (Mitteroecker & Bookstein, 2008). The current data indicate that in the specific case of the highly complex and derived human head, this delicate link is probably related to developmental mechanisms in which one of the modules – the brain – directly influences the development of the surrounding skeletal structures from the other modules, thus assuring a functional global spatial coherence and integrity. In order to test this hypothesis, the plan is to study more cases of human congenital malformation and contrast them with developmental data from non-human model organisms, using recent anatomical network methodology (Esteve-Altava et al. 2015) to build quantitative networks, including the brain and all nerves and musculoskeletal structures of the head. As recent studies have stressed that individuals with T18 and T21 often share some similar phenotypic patterns (Smith et al. 2015), the proposed network modeling study will also have implications for a better understanding of the processes and patterns of Down syndrome development.

Acknowledgments

This research was supported in part by NIH/NIMHD G12 MD007597; MGL is supported by R01AA021262. The authors wish to thank Dr Janine Ziermann for help with staging the control specimens, Dr Duerinckx for access to imaging equipment in the Department of Radiology, and Dr Lee in the Department of Pathology for his support of this research.

References

Alberch P. The logic of monsters: evidence for internal constraint in development and evolution. Geobios. 1989; 22:21–57.

Author Manuscript Author Manuscript Author Manuscript Author Manuscript

Aoto K, Shikata Y, Imai H, et al. Mouse Shh is required for prechordal plate maintenance during brain and craniofacial morphogenesis. Dev Biol. 2009; 327:106–120. [PubMed: 19103193]

Arnold WH, Meiselbach V. 3-D reconstruction of a human fetus with combined holoprosencephaly and cyclopia. Head Face Med. 2009; 5:14. [PubMed: 19563629]

Aruna E, Chakravarthy VK, Rao DN, et al. Holoprosencephaly with multiple anomalies of the craniofacial bones – an autopsy report. J Clin Diagn Res. 2013; 7:1722–1724. [PubMed: 24086891]

Belloni E, Muenke M, Roessler E, et al. Identification of Sonic hedgehog as a candidate gene responsible for holoprosencephaly. Nat Genet. 1996; 14:353–356. [PubMed: 8896571]

Bruns D, Campbell E. Twenty-two survivors over the age of 1 year with full trisomy 18: presenting and current medical conditions. Am J Med Genet A. 2014; 164A:610–619. [PubMed: 24375938]

Carbe C, Garg A, Cai Z, et al. An allelic series at the paired box gene 6 (Pax6) locus reveals the functional specificity of Pax genes. J Biol Chem. 2013; 288:12 130–12 141.

Cereda A, Carey JC. The trisomy 18 syndrome. Orphanet J Rare Dis. 2012; 7:81. [PubMed: 23088440]

Chiang C, Litingtung Y, Lee E, et al. Cyclopia and defective axial patterning in mice lacking Sonic hedgehog gene function. Nature. 1996; 383:407–413. [PubMed: 8837770]

Cohen MM Jr. Malformations of the craniofacial region: evolutionary, embryonic, genetic, and clinical perspectives. Am J Med Genet. 2002; 115:245–268. [PubMed: 12503119]

Couly GF, Coltey PM, Le Douarin NM. The triple origin of skull in higher vertebrates: a study in quail-chick chimeras. Development. 1993; 117:409–429. [PubMed: 8330517]

Deftereou TE, Tsoulopoulos V, Alexiadis G, et al. Congenital disorder of true cyclopia with polydactylia: case report and review of the literature. Clin Exp Obstet Gynecol. 2013; 40:460–462. [PubMed: 24283191]

DeMeyer W, Zeman W, Palmer C. The face predicts the brain: diagnostic significance of median facial anomalies for holoprosencephaly (archinencephaly). Pediatrics. 1964; 34:256–263. [PubMed: 14211086]

England, M. Life before Birth: Normal Fetal Development. St. Louis, MO: Mosby; 1996.

Ericson J, Morton S, Kawakami A, et al. Two critical periods of Sonic Hedgehog signaling required for the specification of motor neuron identity. Cell. 1996; 87:661–673. [PubMed: 8929535]

Esteve-Altava B, Diogo R, Smith C, et al. Anatomical networks reveal the musculoskeletal modularity of the human head. Sci Rep. 2015; 5:8298. [PubMed: 25656958]

Ettema AM, Wenghoefer M, Hansmann M, et al. Prenatal diagnosis of craniomaxillofacial malformations: a characterization of phenotypes in trisomies 13, 18, and 21 by ultrasound and pathology. Cleft Palate Craniofac J. 2010; 47:189–196. [PubMed: 19860526]

Fedorov A, Beichel R, Kalpathy-Cramer J, et al. 3D Slicer as an image computing platform for the Quantitative Imaging Network. Magn Reson Imaging. 2012; 30:1323–1341. [PubMed: 22770690]

Floore C, Robertson A, Samuel I, et al. A pseudoisochromosome 18q and an isodicentric chromosome 18. Clin Genet. 1989; 35:450–454. [PubMed: 2736793]

Garzozi HJ, Barkay S. Case of true cyclopia. Br J Ophthalmol. 1985; 69:307–311. [PubMed: 3922398]

Gravholt CH, Bugge M, Stromkjaer H, et al. A patient with Edwards syndrome caused by a rare pseudodicentric chromosome 18 of paternal origin. Clin Genet. 1997; 52:56–60. [PubMed: 9272714]

Helms JA, Kim CH, Hu D, et al. Sonic hedgehog participates in craniofacial morphogenesis and is down-regulated by teratogenic doses of retinoic acid. Dev Biol. 1997; 187:25–35. [PubMed: 9224671]

Hu D, Helms JA. The role of sonic hedgehog in normal and abnormal craniofacial morphogenesis. Development. 1999; 126:4873–4884. [PubMed: 10518503]

Ingham PW, McMahon AP. Hedgehog signaling in animal development: paradigms and principles. Genes Dev. 2001; 15:3059–3087. [PubMed: 11731473]

Keaton AA, Solomon BD, Kauvar EF, et al. TGIF mutations in human holoprosencephaly: correlation between genotype and phenotype. Mol Syndromol. 2010; 1:211–222. [PubMed: 22125506]

Kietzman HW, Everson JL, Sulik KK, et al. The teratogenic effects of prenatal ethanol exposure are exacerbated by Sonic Hedgehog or GLI2 haploinsufficiency in the mouse. PLoS ONE. 2014; 9:e89448. [PubMed: 24586787]

Author Manuscript Author Manuscript Author Manuscript Author Manuscript

Kish PE, Bohnsack BL, Gallina DD, et al. The eye as an organizer of craniofacial development. Genesis. 2011; 49:222–230. [PubMed: 21309065]

Lang AF, Schlager FM, Gardner HA. Trisomy 18 and cyclopia. Teratology. 1976; 14:195–203. [PubMed: 982315]

Marcucio RS, Cordero DR, Hu D, et al. Molecular interactions coordinating the development of the forebrain and face. Dev Biol. 2005; 284:48–61. [PubMed: 15979605]

Marti E, Takada R, Bumcrot DA, et al. Distribution of Sonic hedgehog peptides in the developing chick and mouse embryo. Development. 1995; 121:2537–2547. [PubMed: 7671817]

Mathers P, Grinberg A, Mahon K, et al. The Rx homeobox gene is essential for vertebrate eye development. Nature. 1997; 387:603–607. [PubMed: 9177348]

McGrath P. The proboscis in human cyclopia: an anatomical study in two dimensions. J Anat. 1992; 181(Pt 1):139–149. [PubMed: 1294563]

Mitteroecker P, Bookstein F. The evolutionary role of modularity and integration in the hominoid cranium. Evolution. 2008; 62:943–958. [PubMed: 18194472]

Moses, KP.; Banks, JC.; Nava, PB., et al. Atlas of Clinical Gross Anatomy. Madrid: Elsevier Mosby; 2005.

Nicolaides KH, Salvesen DR, Snijders RJ, et al. Strawberry- shaped skull in fetal trisomy 18. Fetal Diagn Ther. 1992; 7:132–137. [PubMed: 1503648]

O'Rahilly R, Muller F. Interpretation of some median anomalies as illustrated by cyclopia and symmelia. Teratology. 1989; 40:409–421. [PubMed: 2623629]

Orioli IM, Amar E, Bakker MK, et al. Cyclopia: an epidemiologic study in a large dataset from the International Clearinghouse of Birth Defects Surveillance and Research. Am J Med Genet C Semin Med Genet. 2011; 157C:344–357. [PubMed: 22006661]

Petryk A, Graf D, Marcucio R. Holoprosencephaly: signaling interactions between the brain and the face, the environment and the genes, and the phenotypic variability in animal models and humans. Wiley Interdiscip Rev Dev Biol. 2015; 4:17–32. [PubMed: 25339593]

Powers SE, Taniguchi K, Yen W, et al. Tgif1 and Tgif2 regulate Nodal signaling and are required for gastrulation. Development. 2010; 137:249–259. [PubMed: 20040491]

Raam MS, Solomon BD, Muenke M. Holoprosencephaly: a guide to diagnosis and clinical management. Indian Pediatr. 2011; 48:457–466. [PubMed: 21743112]

Rasmussen M, Jacobsson M, Bjorck L. Genome-based identification and analysis of collagen-related structural motifs in bacterial and viral proteins. J Biol Chem. 2003; 278:32 313–32 316.

Reid S, Ziermann JM, Gondré-Lewis MC. Genetically induced abnormal cranial development in human trisomy 18 with holoprosencephaly: comparisons with the normal tempo of osteoneural development. J Anat. 2015; 227:21–33. [PubMed: 26018729]

Richtsmeier JT, Flaherty K. Hand in glove: brain and skull in development and dysmorphogenesis. Acta Neuropathol. 2013; 125:469–489. [PubMed: 23525521]

Roessler E, Belloni E, Gaudenz K, et al. Mutations in the human Sonic Hedgehog gene cause holoprosencephaly. Nat Genet. 1996; 14:357–360. [PubMed: 8896572]

Roessler E, El-Jaick KB, Dubourg C, et al. The mutational spectrum of holoprosencephaly-associated changes within the SHH gene in humans predicts loss-of-function through either key structural alterations of the ligand or its altered synthesis. Hum Mutat. 2009; 30:E921–E935. [PubMed: 19603532]

Rosa RF, Trevisan P, Rosa RC, et al. Trisomy 18 and neural tube defects. Pediatr Neurol. 2013; 49:203–204. [PubMed: 23831245]

Rubenstein JL, Beachy PA. Patterning of the embryonic forebrain. Curr Opin Neurobiol. 1998; 8:18–26. [PubMed: 9568388]

Smith DW, Patau K, Therman E, et al. A new autosomal trisomy syndrome: multiple congenital anomalies caused by an extra chromosome. J Pediatr. 1960; 57:338–345. [PubMed: 13831938]

Smith, CM.; Molnar, J.; Ziermann, JM., et al. Muscular and Skeletal Anomalies in Human Trisomy in an Evo-Devo Context. Oxford: CRC Press; 2015.

Author Manuscript Author Manuscript Author Manuscript Author Manuscript

Solomon BD, Mercier S, Velez JI, et al. Analysis of genotype– phenotype correlations in human holoprosencephaly. Am J Med Genet C Semin Med Genet. 2010; 154C:133–141. [PubMed: 20104608]

Steding G, Jian Y. The origin and early development of the nasal septum in human embryos. Ann Anat. 2010; 192:82–85. [PubMed: 20149609]

Taniguchi K, Anderson AE, Sutherland AE, et al. Loss of Tgif function causes holoprosencephaly by disrupting the SHH signaling pathway. PLoS Genet. 2012; 8:e1002524. [PubMed: 22383895]

Tank, PW. Grant's Dissector. 15th. Walters Kluwer: Lippincott Williams & Wilkins; 2013.

Wall NA, Hogan BL. Expression of bone morphogenetic protein-4 (BMP-4), bone morphogenetic protein-7 (BMP-7), fibro-blast growth factor-8 (FGF-8) and sonic hedgehog (SHH) during branchial arch development in the chick. Mech Dev. 1995; 53:383–392. [PubMed: 8645604]

Young NM, Chong HJ, Hu D, et al. Quantitative analyses link modulation of sonic hedgehog signaling to continuous variation in facial growth and shape. Development. 2010; 137:3405–3409. [PubMed: 20826528]

Author Manuscript
Author Manuscript
Author Manuscript
Author Manuscript

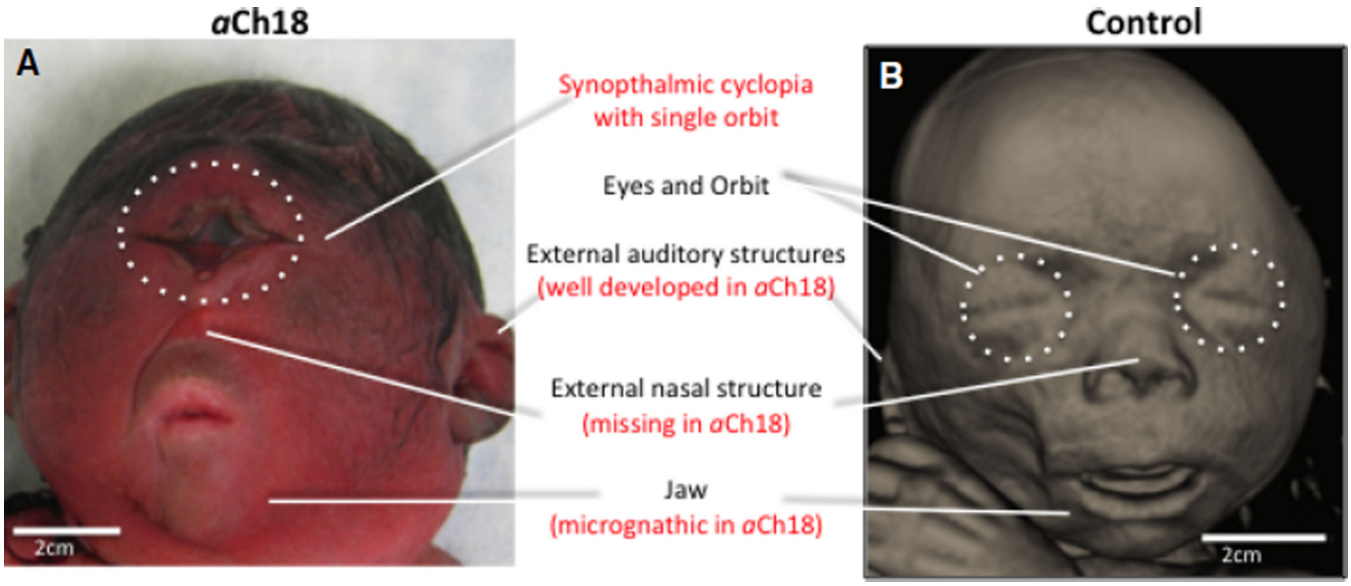

Fig. 1.

Superficial view of the facial features of a cyclopic HPE fetus and age-matched control. (A) Macroscopic view of the 28-week T18-like aberrant Ch18 (*a*Ch18) fetus with a fused orbit, missing nasal structure, micrognathic jaw and well-developed external auditory structures. (B) 3D reconstruction of CT slices of age-matched control fetus showing appropriate development of superficial face at 29 weeks of gestation.

Author Manuscript Author Manuscript Author Manuscript Author Manuscript

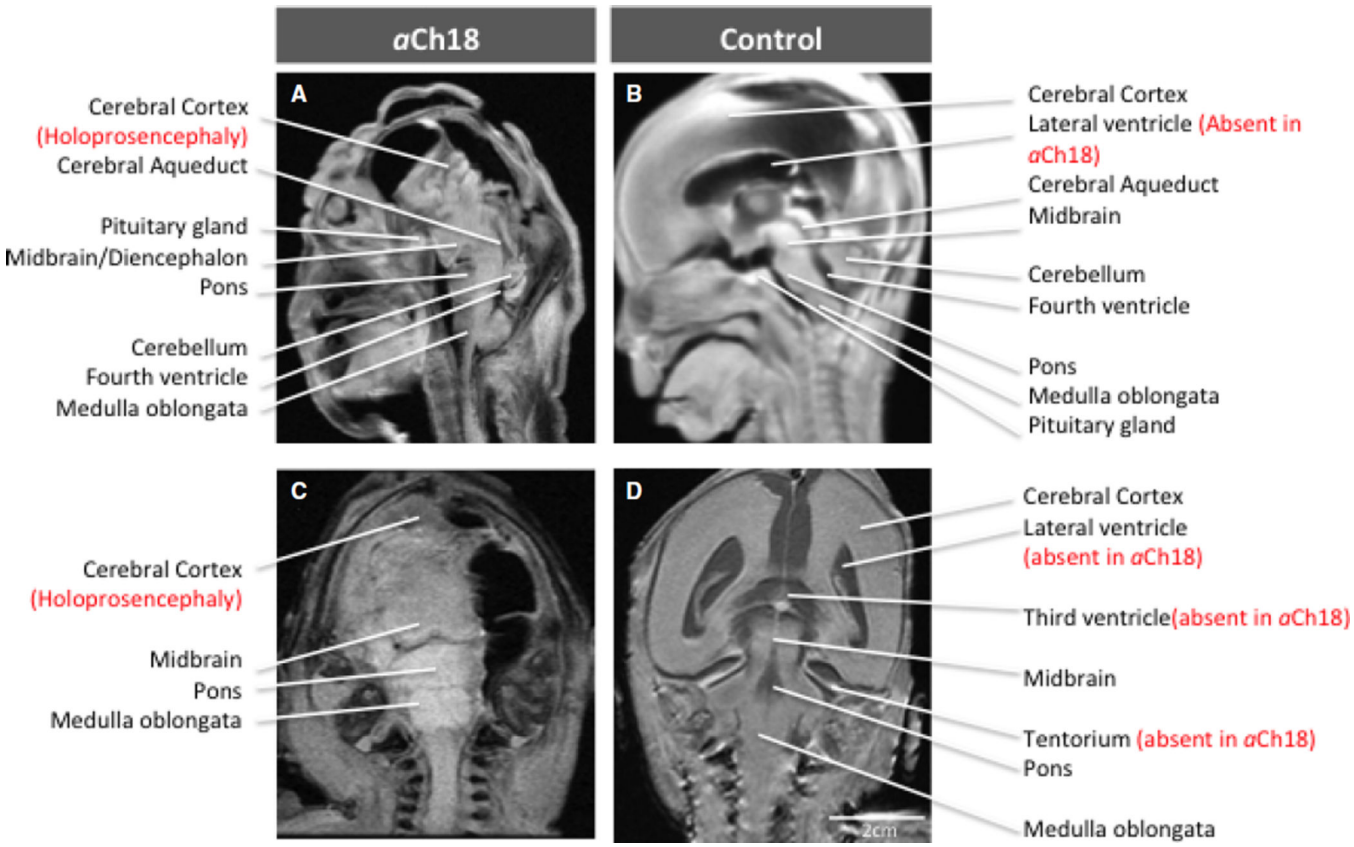

Fig. 2.

MRI phenotypic presentation of HPE in individual brain structures. (A) Sagittal view of HPE brain in aberrant Ch18 (*a*Ch18), with features of anencephaly, absent anterior cranial fossa, and upright, enlarged brainstem structures. The control fetus (B) has a fully induced forebrain and well-developed lateral ventricle, which are both missing in *a*Ch18. Coronal slice of *a*Ch18 showing missing brain tissue on the right and lack of separation in the lobes (alobar). (D) The control for (C) exhibits the ventricles missing in *a*Ch18, and the classic morphology of the brainstem.

Author Manuscript Author Manuscript Author Manuscript Author Manuscript

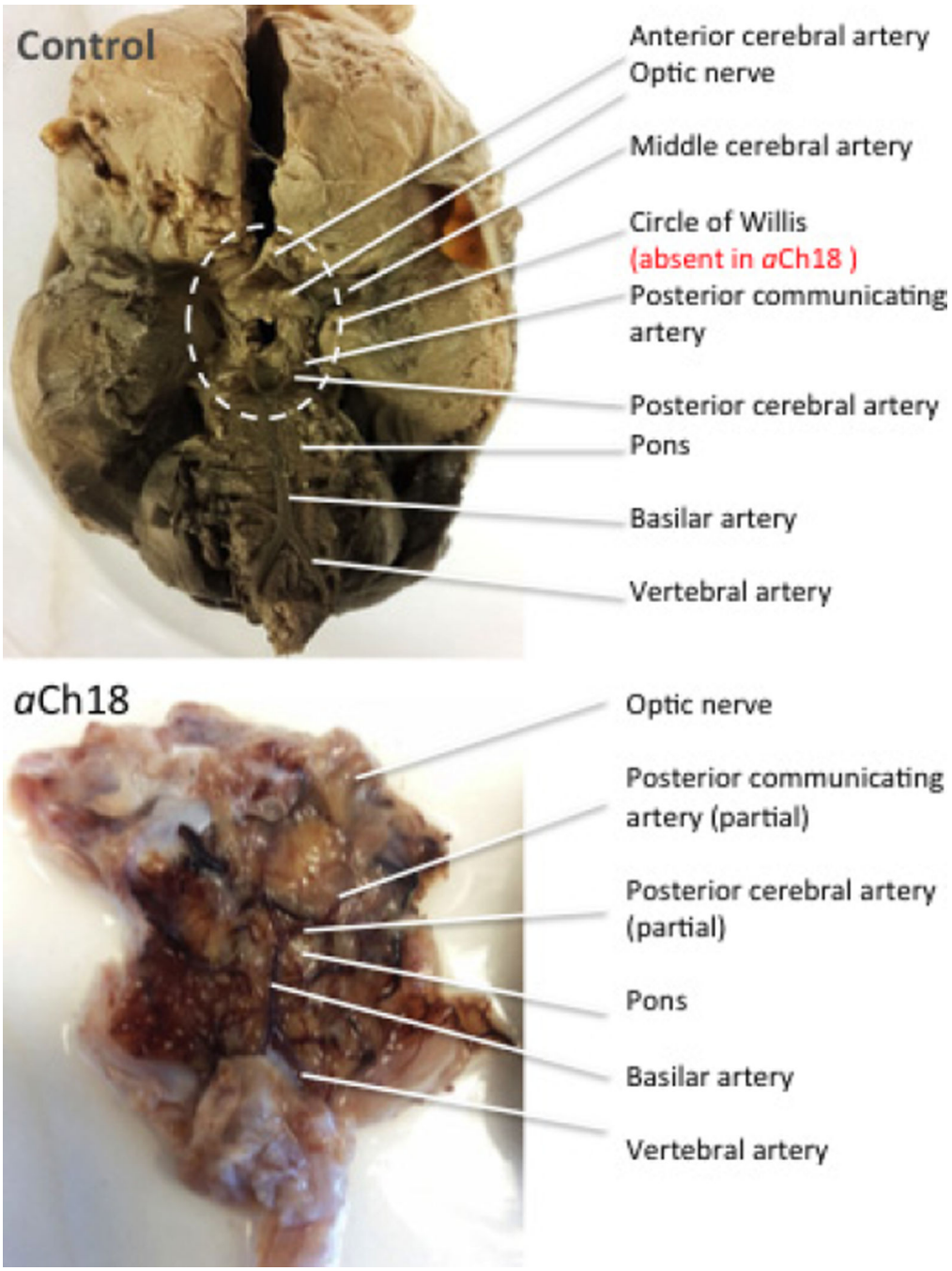

Fig. 3.

Arterial supply to the brain mimics the neural defects. This ventral view of aberrant Ch18 (*a*Ch18; left) and control (right) brain shows the presence of bilateral vertebral arteries and a central basilar artery in *a*Ch18, but the anterior components that comprise the Circle of Willis are absent.

Author Manuscript Author Manuscript Author Manuscript Author Manuscript

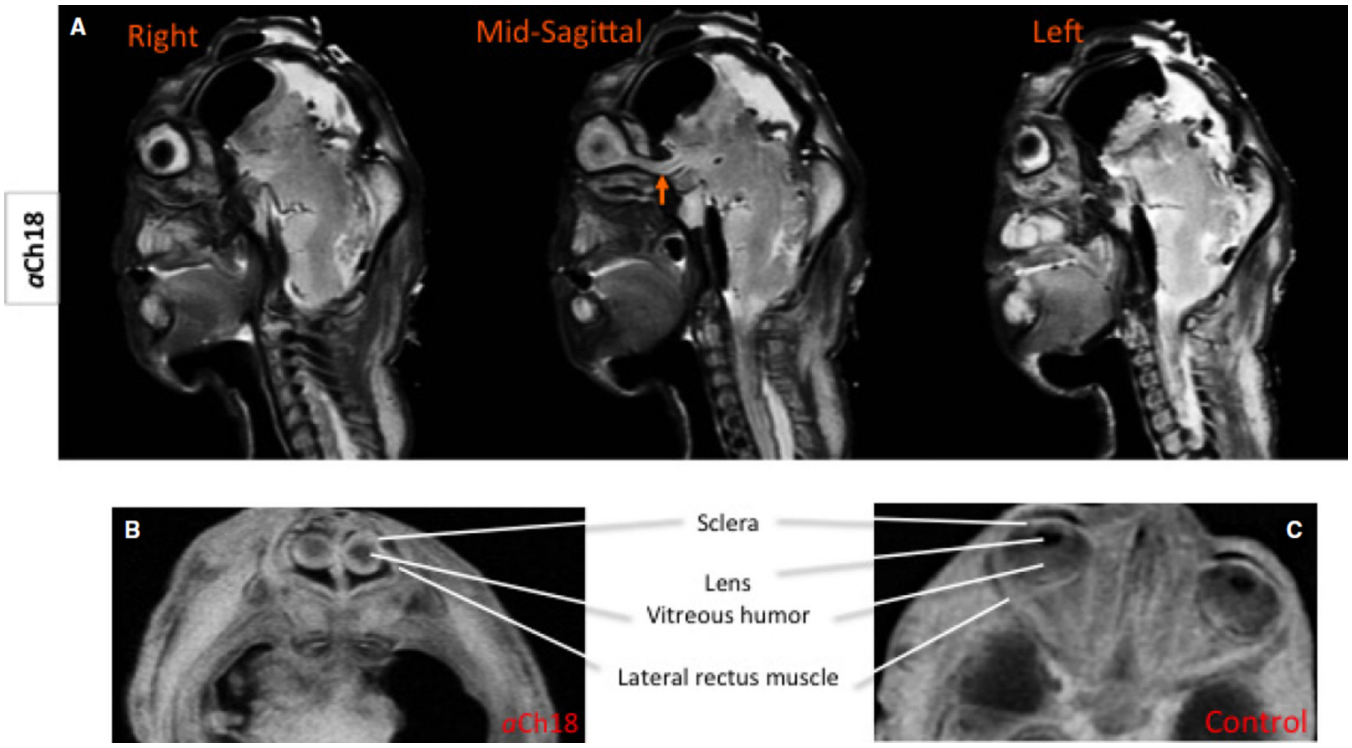

Fig. 4.

Eye structures in the *a*Ch18 synophthalmic cyclops analysed with MRI. (A) Sagittal slices of the *a*Ch18 fetus from right to left through the midline showing a fused optic nerve midsagitally (arrow); T2 weighted (B) horizontal slice through the mid-ocular region demonstrating the absence of the lens, and the presence of some extraocular muscles. (C) The control for (B) shows the normally developed intrinsic ocular structures at 29 weeks. (B and C) T1-weighted MRIs. Arrow demarcates medially located single optic nerve.

Author Manuscript Author Manuscript Author Manuscript Author Manuscript

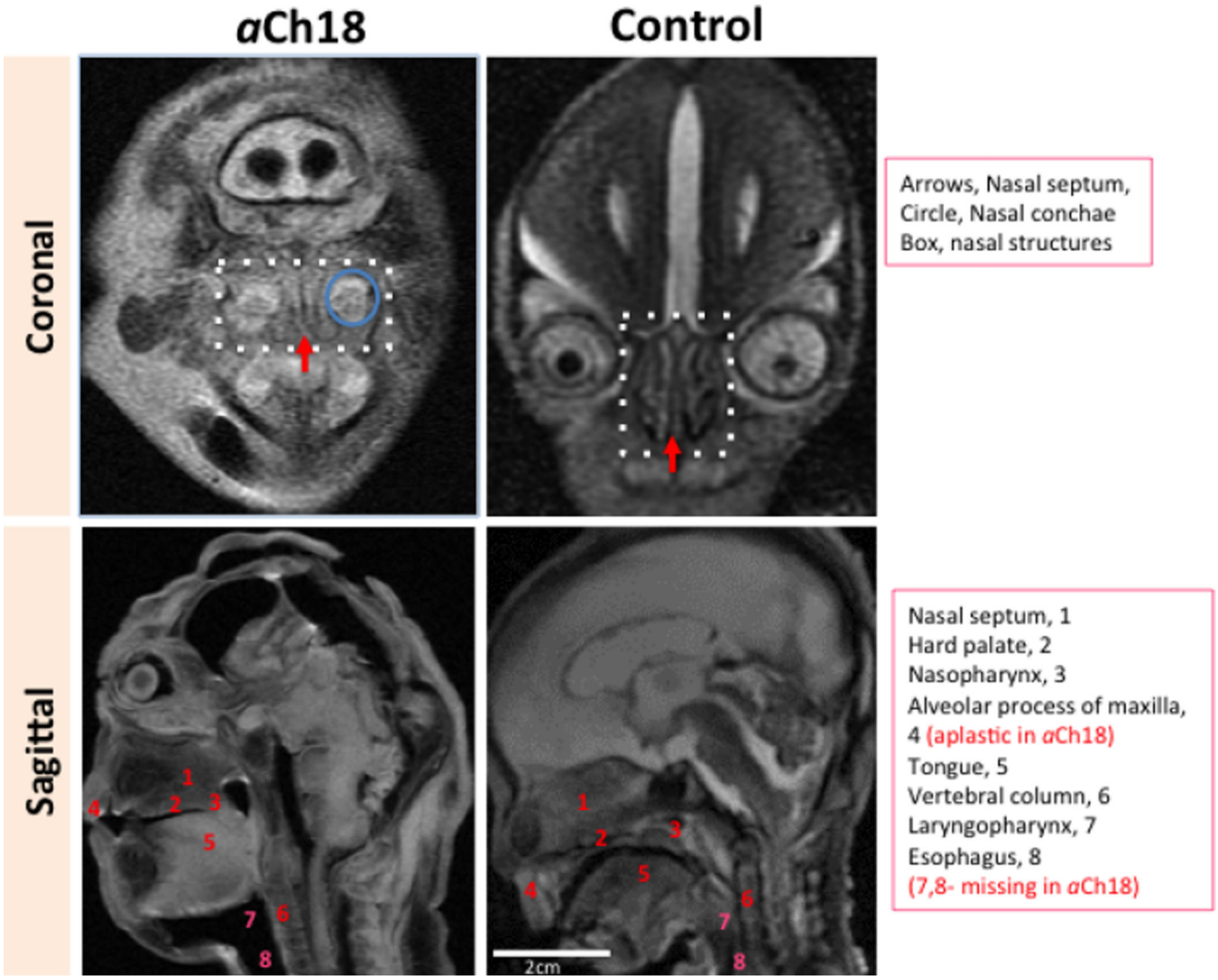

Fig. 5.

Internal nasal structures but no pharyngeal structures in aberrant Ch18 (*a*Ch18) specimen. Coronal (upper panels) and sagittal (lower panels) T2-weighted MRI sections exhibit many nasal structures in the *a*Ch18 (left) as compared with controls (right). The alveolar process of the maxilla is undeveloped, along with the esophagus and most of the structures of oropharynx and laryngopharynx in the *a*Ch18.

Author Manuscript Author Manuscript Author Manuscript Author Manuscript

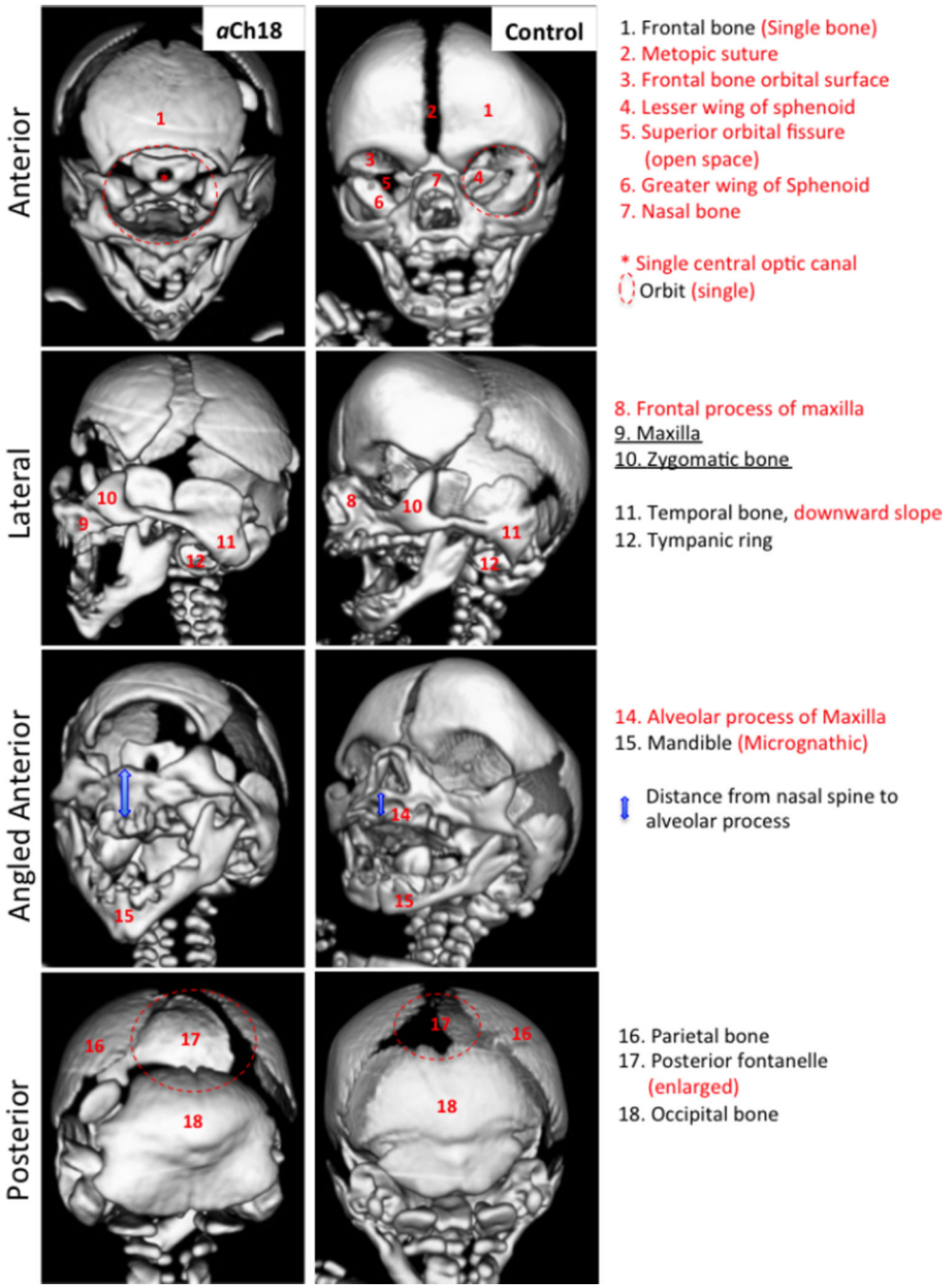

Fig. 6.

Craniofacial features of bone in aberrant Ch18 (*a*Ch18) fetus compared with control. 3D reconstructed CT scans of a 28-week old *a*Ch18 (left column) vs. a 29-week control fetus. Anterior (1st row), lateral (2nd row), angled anterior (3rd row) and posterior (4th row) perspectives of the cranium. Lateral features are preserved, whereas medial structures are severely impacted. Red lettering indicates an absence or abnormality in *a*Ch18.

Author Manuscript Author Manuscript Author Manuscript Author Manuscript

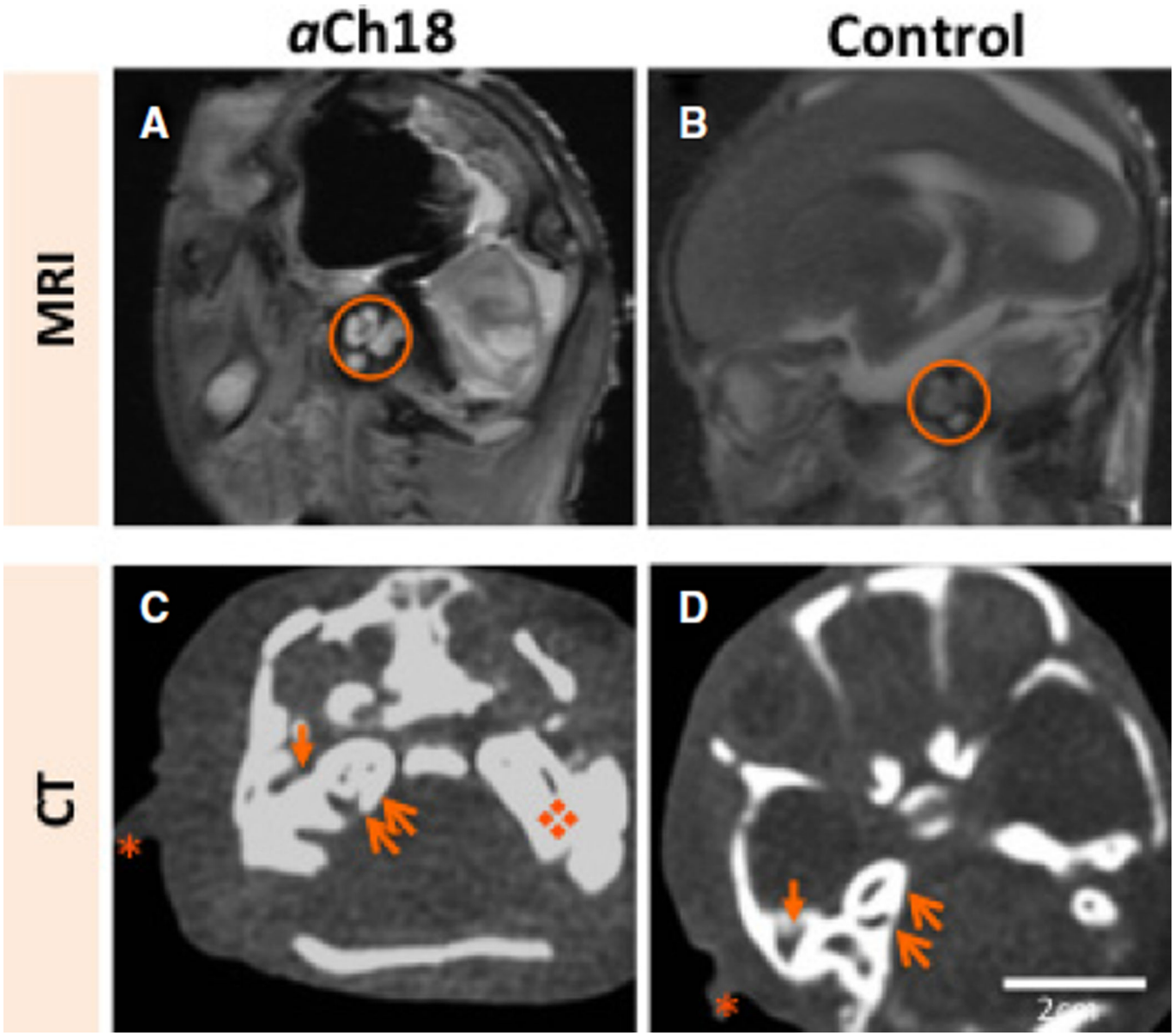

Fig. 7.

Internal, middle and external auditory structure development in HPE and cyclopia. (A) Sagittal magnetic resonance imaging (MRI) of the lateral head of an aberrant Ch18 (*a*Ch18) fetus showing the middle auditory structures, mainly the ossicles (circle) appearing radiodense in *a*Ch18 compared with (B) the age-matched control. (C) Horizontal section of the head at the level of the inner and external ear, and the petrous temporal bone showing their presence in radiodense form compared with (D) the age-matched control. Asterisk, pinna of ear; thin arrow, cochlea; thick arrow, external ear canal; diamond, enlarged petrous temporal bone. CT, computed tomography.

Author Manuscript Author Manuscript Author Manuscript Author Manuscript

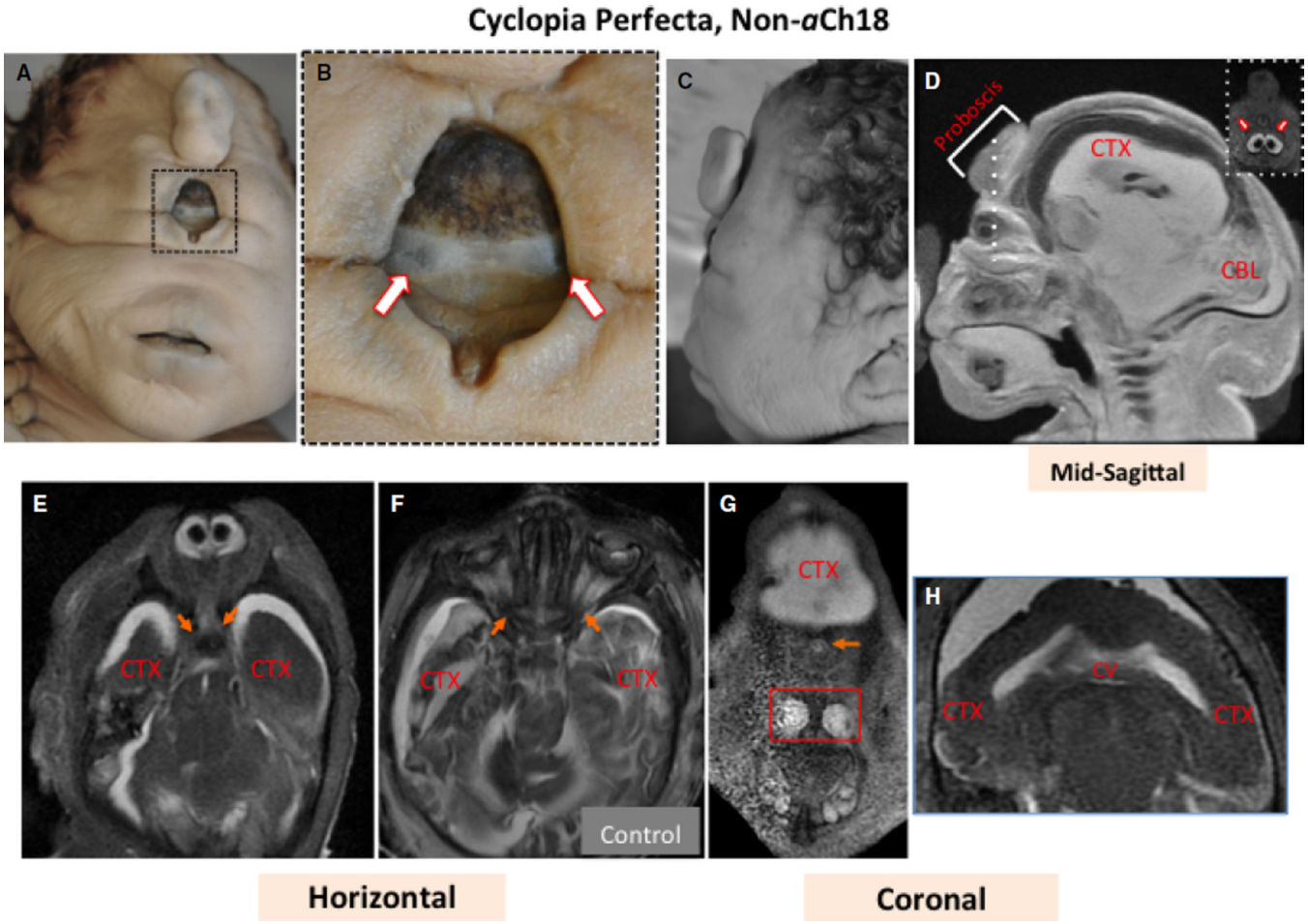

Fig. 8.

Superficial and MRI analysis of craniofacial features of a 35-week non-aberrant Ch18 (*a*Ch18) cyclopic fetus with normal karyotype. (A, B) Frontal views of the 35-week cyclops with (B) enlargement of the eye to reveal two globes (arrows). (C) A lateral view of the head. (D) Sagittal, (E) horizontal, and (G and H) coronal sections through the head and face. (F) Age-matched control. The dashed line in (D) shows the plane of inset at the right. Arrows in (E) show bifurcating nerves as they enter the brain laterally. Arrows in (F) show nerves originating from two optic globes for normal binocular vision. The arrow in (G) shows a single optic nerve centrally, and the box reveals nasomaxillary structures. (H) A single cerebral ventricle (CV) in white connected at the midline, and unseparated cerebral cortex (CTX). CTX appears dark or light depending on if the images were, respectively, acquired with T1 or T2 weighting.

Author Manuscript
Author Manuscript
Author Manuscript
Author Manuscript

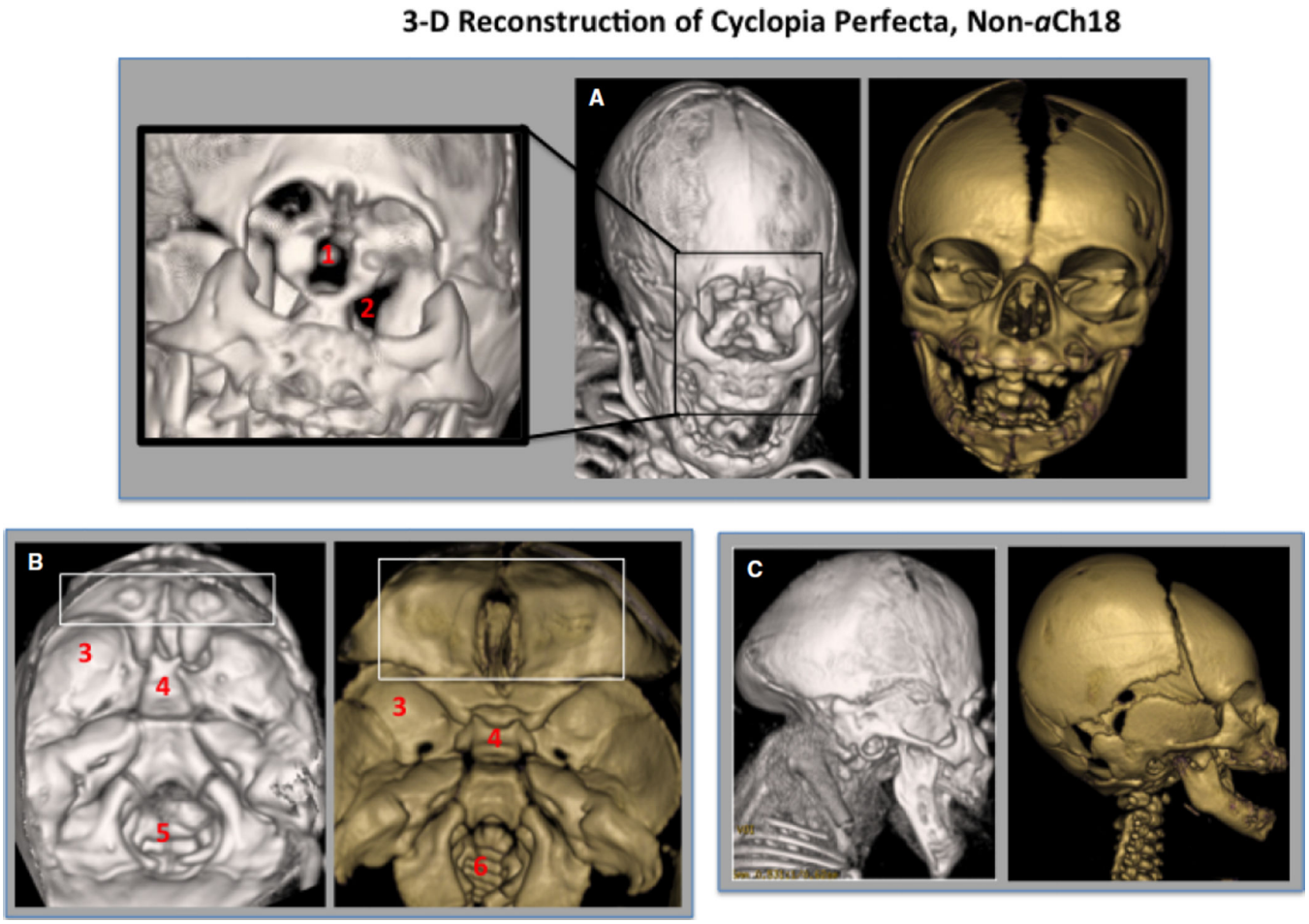

Fig. 9.

Analysis of the external cranium and internal floor of the cranium of a 35-week non-aberrant Ch18 (*a*Ch18) cyclopia perfecta fetus in 3D. (A) Frontal view of the reconstructed face of cyclops (gray) with magnification at left showing defect in the orbit with a central slit for the optic nerve (1), but with lateral formation of a widened superior orbital fissure (2) compared with non-cyclopic control (gold). (B) Interior of the cranium with a small orbital plate of frontal bone with no crista galli (box) and anteriorly shifted middle cranial fossa (3), immature deviated sphenoid bone, and enlarged foramen magnum and petrous temporal bone. (C) Lateral aspect of the cranium, with unremarkable maxillary and mandibular structures, but with cranial defects in the temporal/occipital bones as well as abnormal cervical and thoracic vertebrae. Gray, 35-week cyclops; Gold, newborn control.

Author Manuscript Author Manuscript Author Manuscript Author Manuscript

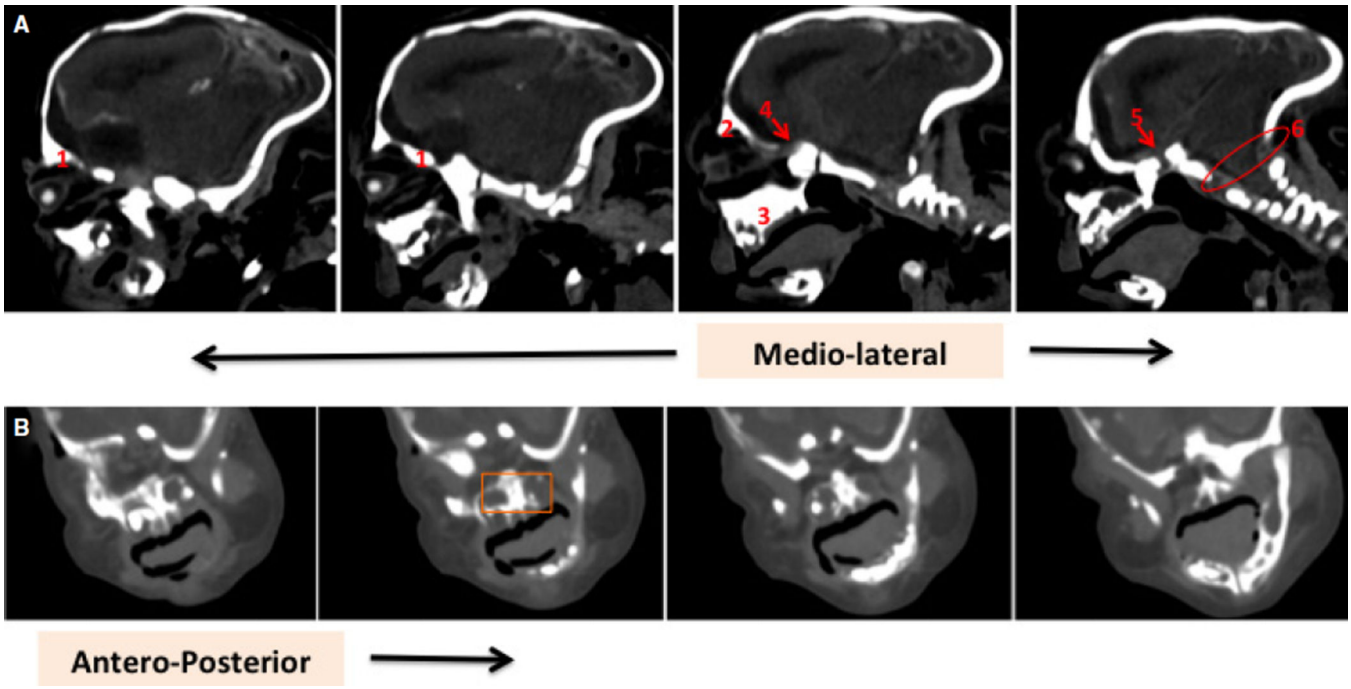

Fig. 10.

Single CT slice analysis of facial features of the non *a*Ch18 cyclopia perfecta fetus at 35 weeks. (A) Adjacent mediolateral sections to emphasize the presence of the (1) orbital plate of frontal bone, (2) frontal process, (3) nasal septum, (4) centrally located optic nerve, (5) pituitary (appears gray surrounded by white sella turcica of the body of the sphenoid) and (6) enlarged foramen magnum. (B) Anteroposterior sections are shown to emphasize centrally located nasal structures, including radiodense septum/conchae, and radiolucent maxillary sinuses on either end.